Preliminary Characterization of a Diverging Cusped Field (DCF) Thruster

IEPC-2009-166

Presented at the 31st International Electric Propulsion Conference,
University of Michigan • Ann Arbor, Michigan • USA
September 20 – 24, 2009

Christopher V. Young,[1] Andrew W. Smith,[2] and Mark A. Cappelli,[3]
High Temperature Gasdynamics Laboratory, Stanford University, Stanford, CA 94305-3032, USA

Abstract: An initial characterization of a diverging cusped field (DCF) thruster with a straight (non-diverging) discharge channel is presented. The thruster is operated on krypton propellant, at power levels ranging from 25-250 W. Thrust, specific impulse, and thrust (anode) efficiency are found to be very sensitive to cathode placement, and thrust efficiencies exceeding 20% are found over a range of operating conditions. This thruster appears to be unusually quiescent, with small amplitude (<1%), high frequency (100 kHz) fluctuations in discharge current. Plume ion current measurements indicate the existence of a conical ion emission, similar to that seen previously in a model with diverging channel walls; this suggests that the ion divergence of the plume is more closely connected to the magnetic field topography than the channel geometry. When operating with 300 V to the anode, plasma potential measurements throughout the near field reveal regions of elevated plasma potential (in some places exceeding 100 V) that are coincident with the most luminous visible regions of the discharge, where the highest ion current densities are found. In contrast, the plume electron temperature is found to peak (at more than 10 eV) along the central axis.

Nomenclature

B_{max}	=	maximum magnitude of magnetic field along a field line
B_{min}	=	minimum magnitude of magnetic field along a field line
e	=	fundamental charge
I_a	=	anode current
I_b	=	beam current
I_{sp}	=	specific impulse
j	=	collected current density
k	=	Boltzmann's constant
$\dot{m}$	=	mass flow rate
m_e	=	electron mass
m_i	=	ion mass
P_a	=	anode power
r	=	cathode radial position
R	=	distance from Faraday probe to thruster exit plane
T	=	thrust
T_e	=	electron temperature
V_a	=	anode potential
V_{probe}	=	emissive probe potential output

[1] Undergraduate Research Assistant, Mechanical Engineering Department, cvyoung@stanford.edu.
[2] Graduate Research Assistant, Mechanical Engineering Department, awsmith@stanford.edu.
[3] Professor, Mechanical Engineering Department, cap@stanford.edu.

z = cathode axial position
η_a = anode thrust efficiency
φ = angle of Faraday probe relative to thruster axis
φ_c = cold probe (sheath) potential
φ_h = hot probe (plasma) potential
φ_p = plasma potential

I. Introduction

THE growing interest in the miniaturization of spacecraft is fueling increased development of low power electric propulsion. Yet, there are only relatively few plasma propulsion technologies that can currently service this regime. One such device is the Hall thruster; however, as operating powers decrease these thrusters appear to suffer a severe degradation of performance. Hall thrusters that operate nominally at 200 W have demonstrated anode efficiencies in the 40% range,[1] although the efficiencies drop dramatically below 100 W.[2] One reason for this diminished performance is heat loading of the center pole piece, which seems to experience significant electron bombardment. Another is the poorly understood scaling of cross-field transport, which meters the flow of electrons to the anode. Clearly, future advances in efficient, sub-100W Hall thrusters depend upon successfully addressing these issues.

One method of avoiding the vulnerabilities of the central pole piece is to remove it altogether, as done in the Cylindrical Hall Thruster (CHT).[3,4] Of course, this comes at the cost of losing certain controls over the shape of the magnetic field. The CHT preserves the cross-field structure for metering electron flow to the anode, and thus retains the essential character of a Hall thruster. In addition, the cylindrical design, coupled with the introduction of magnetic cusps for partial electron mirroring from the walls, increases the electron residence time in regions downstream of the anode trap. These magnetic structures create efficient ionization regions, helping to maintain performance at lower power. The CHT has demonstrated anode efficiencies ranging from about 20-28% between 100 and 200W.[5]

Recently, researchers at the Massachusetts Institute of Technology (MIT) revisited the idea of using a series of cusps to magnetostatically trap electrons in a cylindrical discharge cavity.[6,7] This design departs from traditional Hall thrusters, as the characteristic cross-field region upstream of the anode is eliminated entirely. Rather, the anode is placed in regions of magnetic field convergence along the thruster axis, at the base of the discharge channel. In utilizing permanent magnets, the design sacrifices the ability to meter electron flow to the anode via in-situ tuning of the magnetic field. This is accomplished instead by manipulating the magnetic mirror ratio through a combination of design parameters: the anode position relative to the magnetic field, the shape of the outer magnetic cusps, and the interior region within these cusps where electrons collide with the ceramic insulator lining the channel. In the MIT design, the overall magnetic field strength diminishes along the centerline, with the series of three magnetic cusps following the diverging conical channel downstream of the anode. The geometry of the channel, coupled with its unique magnetic field structure, has led to its description as the Diverging Cusped Field (DCF) Thruster. Preliminary performance testing[8] suggests that this thruster operates with an anode thrust efficiency in excess of 40% in the 200 W range – an exciting result, especially given its largely un-optimized operation and notable lack of the inherent vulnerabilities plaguing Hall thrusters operating in the low power regime.

In this paper, we present a study of a smaller DCF variant with straight, rather than diverging, channel walls. The magnetic field structure is qualitatively similar to the MIT DCF thruster, with stronger cusps located closer to the anode and a diminishing field downstream along the axis. However, the discharge channel is cylindrical, and does not follow the contours of the magnetic field lines extending out into the plume. In this way, we attempt to separate the role played by the diverging channel from that of the diverging field lines within the channel. As described below, we find that the resulting thruster behavior, including the ion plume current, is qualitatively similar to that of the MIT design. We also find that the straight channel and reduction in size do not significantly compromise performance, and consistent anode efficiencies near 23% are obtained when operating with krypton as a propellant at power levels as low as 40 W. The thruster described here is operated over a range of anode powers extending to 240 W, and its performance is found to strongly depend on the location and orientation of the cathode. This DCF thruster also exhibits certain irreproducible modes of operation that drastically affect its performance both beneficially and detrimentally.

II. Experiment

A. Experimental Facility and Diagnostics

The thruster was operated in the Stanford Plasma Physics Laboratory (SPL) vacuum facility, which consists of a stainless steel chamber 4 m long and 1.25 m in diameter. The chamber utilizes a two-stage cryogenic cooling system: the first stage consists of a shroud that is cooled using a Polycold Fast Cycle Water Vapor Cryopump (PFC, model 1100), and the second stage is a cryopanel cooled to 14 K using a closed-loop cryogenic helium refrigerator. The background pressure is maintained at ~1 x 10^{-6} Torr (measured using an ion gauge) during nominal thruster operation.

The discharge is powered with a Sorenson DCS-600-1.7 DC power supply, operated in voltage-limited mode, with the cathode (Ion Tech Model HCN-252) heater and keeper maintained on separate DC power supplies. Figure 1 shows a schematic diagram of the chamber and associated circuitry. During operation, the discharge current of the thruster is monitored by measuring the voltage drop across a 1 Ω resistor (placed in series between the anode and power supply, see Fig. 1) using a differential voltage probe. The resulting power reaching the discharge is taken to be the product of the discharge current and discharge voltage (as indicated on the power supply, leading to a ~1% overestimation of the discharge power due to the discounted potential drop across the resistor).

The propellant feeds to the thruster and cathode are metered using two mass flow controllers (MFCs): a 5 sccm UNIT UFC-1201A for the cathode gas (argon) and a 100 sccm UNIT UFC-1200A for the anode gas (krypton). The flow controllers are calibrated for each gas by measuring the instantaneous pressure and temperature in a test cell of known volume at a given (reported) flow rate by the MFC. By measuring the rate of pressure and temperature increase (the latter usually being negligible), an "actual" flow rate may be calculated through the ideal gas law and compared against the "reported" value. Known linear conversion factors between calibration gases (as reported by the manufacturers) are taken as guidelines, but do not exactly match our calibrations. A linear relationship between actual and reported flow for argon is found for both controllers, while a slightly non-linear one is found for krypton.

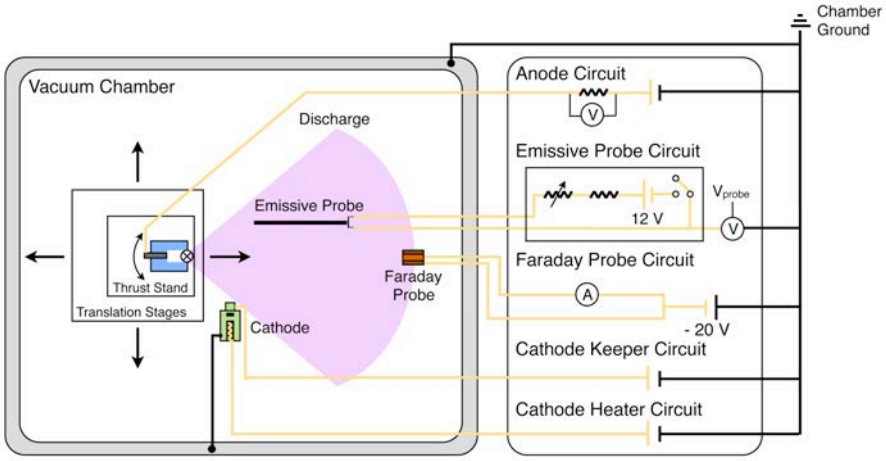

Figure 1. Schematic of experimental setup and associated circuitry.

The thruster is mounted on an inverted-pendulum-type thrust stand (shown schematically in Ref. 9), with the lower portion mounted to a pair of orthogonal translation stages capable of 20 cm of relative motion at speeds of 1-3 cm/s. The thruster is mounted to the upper portion of the thrust stand (electrically floating) on a rotating translation stage with axis of rotation orthogonal to the two translation stages already mentioned. The two components of the pendulum are connected by four thin flexures, a restoring spring, the calibration system, and propellant gas feed and electrical power lines. An electromagnetic damper is utilized to reduce transient oscillations in the thrust stand induced by vibrations in the environment. A linear voltage differential transformer (LVDT) (Macro Sensors, model PR 812) converts the spatial displacement of the thrust stand to a voltage, which is monitored at 10 Hz using an Agilent data acquisition system. The thrust stand is leveled (i.e. kept horizontal) and water-cooled to reduce drift induced by creep of the coupling components and thermal expansion of the structure, respectively.

The thrust stand calibration is performed using a series of three weights attached to a chain, one end of which is attached to the upper pendulum of the thrust stand via a pulley. The other end of the chain is wound around a spool and is released remotely using a stepper motor. The motor raises and lowers the masses, deflecting the inverted pendulum; the result is a linear displacement versus calibration force curve. However, this system is imperfect due to two primary factors: the effect of the weight of the chain to which the weights are fixed is difficult to precisely quantify, and the axis of the calibration force, while parallel to, is not in line with the discharge central axis. An additional calibration method is employed to reduce such uncertainties in the thrust measurements. A thin nylon fiber is attached to the front of the thruster (post-testing) and draped over a smooth plastic rod such that the fiber is

aligned with the central axis of the thruster. The fiber and the rod are lubricated with a fine boron nitride powder. Weights are attached to the loose end of the fiber, and the resulting displacement of the thrust stand is measured. To reduce frictional effects, the nylon fiber is initially placed slightly off-axis on the lubricated rod, which is then vibrated until the string settles along the central axis. The load is then removed from the thruster, and the unloaded displacement is measured. This pair of measurements is repeated three times for each of three different masses. The masses are then measured using a Mettler AE 240 scale (accurate to 10 μg, a precision of order 10^{-4} for the typical masses utilized). The mass of the nylon fiber is also measured and is generally less than 2% of the total mass. This method thus provides an alternative calibration of thrust force versus linear displacement (voltage) of the inverted pendulum stand. The alternative calibration is believed to provide a more precise measure, and has proved to yield significantly different results than the initial calibration, possibly due to the elimination of torque effects. The system is capable of resolving thrusts to a precision of 0.1 mN, or about 2% of the overall thrust.

During thruster operation, the LVDT output is measured as each of the three chain-mounted weights is transferred to the upper pendulum. The discharge is then turned off and the procedure repeated. The difference between the LVDT output when the discharge is on/off, along with the calibration curve, yields the measured thrust. In the "off" state, gas is still flowing from the thruster and the cathode; however, these effects have been measured to amount to less than 3% of the total thrust.

The potential distribution throughout the near-field of the discharge is measured using a floating emissive probe described in more detail elsewhere.[10] The emitting portion of the probe consists of a 2 mm diameter loop of 150 μm diameter thoriated-tungsten (1%) wire, encased in a 2.5 mm diameter alumina tube serving as the probe body. Direct current (dc) can be driven through the probe, and its floating potential is recorded using a digital oscilloscope (see "V_{probe}" in the Emissive Probe Circuit shown in Fig. 1). The probe is mounted on a translation stage (orthogonal to the two axial translation stages controlling thruster position) allowing for relative motion between the probe and the discharge in 3D. The basic theory of emissive probe characteristics is reasonably well established.[11] A thermionic electron-emitting filament in a low-temperature plasma will float at a potential which approaches the plasma potential when the emitted electron current is sufficiently high (i.e. the filament is sufficiently heated) to neutralize the plasma sheath. The saturation heating current varies slightly with each probe (due to differences in construction), and in the current study we have found that saturation is achieved in all regions of the near-field sampled when the probe is heated with a current of 2.5 A. We take the floating potential of the probe when heated with 2.5 A of current to be the plasma potential. While this introduces a systematic uncertainty in the extracted plasma potential of a few volts, it is considered to be a reasonable tradeoff: it allows us to rapidly acquire the potential by translating the probe over three-dimensional space at a constant probe heater current. The discharge current is monitored during the tests, and the average current is found to vary by less than 0.5% for all of the points tested, regardless of the probe position relative to the thruster.

The unheated (floating) potential is mapped throughout the near-field, taking care to rapidly move the probe in and out of regions of strong heating (such as very near the exit plane) so that it does not become self-emitting. At each measurement location, the probe is paused for one second (to allow any small residual vibrations induced by the translation stages to dampen out), after which the oscilloscope records 50,000 temporal measurements of the probe signal and discharge current simultaneously. These transient measurements are recorded at 20 ns intervals (spanning 1 ms). After the near-field floating potential measurements are complete, the probe current is raised to 2.5-2.6 A, and the measurements are repeated to obtain the plasma potential.

Determining the electron temperature, T_e, from the floating potential measured by the hot and cold probe requires a model of the collected electron and ion current.[10,12] We take:

$$T_e = \frac{2e\left(\varphi_h - \varphi_c\right)}{k\ln\left(m_i/2\pi m_e\right)} \tag{1}$$

where e is the fundamental charge, k is Boltzmann's constant, m_i is the ion mass (in this case krypton), m_e is the electron mass, ϕ_h is the floating potential measured by the probe while in the emissive, hot state, and ϕ_c is the potential measured by the probe in the unheated, cold state. Equation (1) yields a result with an uncertainty of at least ±17% on the measured temperature, attributable alone to the uncertainty in ion collection models.[12]

Finally, ion current density measurements are obtained with a nude faraday probe (or guarded ion probe) similar in construction to that utilized by Hofer et al.[13] The probe has a collector that is 1.11 cm in diameter with a collection area of 0.97 cm^2. The collector and guard ring are both biased to -20 V relative to chamber ground to repel the plume electrons, and the resulting ion current reaching the collector is measured using a picoammeter.

When the ion current is measured, the probe is held fixed in space while the thruster is rotated about an axis passing through the intersection of the exit plane with the central axis of the thruster (see Fig. 1; the axis of rotation is indicated by a circled "X") .

B. Thruster

The Stanford DCF thruster is housed in a 6.10 cm outer diameter, 4.78 cm inner diameter aluminum cylinder that is 7.04 cm in length with the base plate attached (see schematic in Fig. 2). The partially threaded, 0.64 cm diameter graphite anode is kept electrically insulated from the floating aluminum body and plasma discharge with various boron nitride insulators and an alumina sleeve, with only a circular area of 1.29 cm^2 left exposed to the main channel. The magnetic cusped profile (indicated with gray lines on Fig. 2) is created by three samarium cobalt permanent magnets of decreasing height placed same pole-to-pole, and shaped by various 1018 steel components. Boron nitride risers of 0.32 cm height allow the magnetic mirror ratio to be controlled through the anode position relative to these magnetic field lines. The current position is chosen such that the field lines from the lower magnetic cusp are orthogonal to the surface of the anode, yielding a typical mirror ratio (B_{max}/B_{min}) of 1.6. Krypton propellant is injected through a 0.32 cm diameter stainless steel gas line into the propellant channel, where it is distributed evenly into the main discharge channel through a 316 steel diffuser ring with 10 μm pores. The cylindrical discharge channel is 3.97 cm in length and 1.43 cm in diameter, an 88% reduction in enclosed channel volume from the MIT DCF thruster. The slightly diverging geometry at the exit plane of the thruster ensures that field lines from the cathode area (and therefore electron trajectories) point into the main channel, rather than impacting only against the exterior front plane of the thruster.

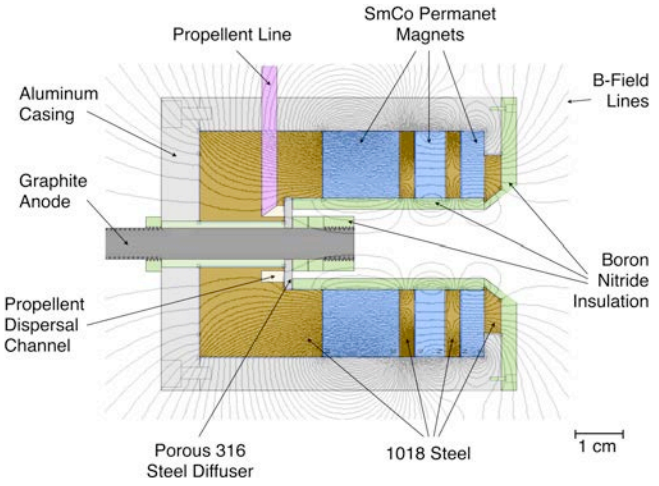

Figure 2. DCF Thruster schematic to scale. Magnetic field lines superimposed from Finite Element Method Magnetics (FEMM) simulation.

The governing principles of the DCF thruster operation are similar in some ways to those utilized by traditional Hall thrusters and the CHT. An electron-emitting cathode (or neutralizer) is positioned outside of the exit plane of the thruster. Some electrons emitted by the external cathode migrate along magnetic field lines down into the thruster channel to service the discharge, while the remainder are expelled to neutralize the ion plume. The series of magnetic cusps within the thruster trap incoming electrons between them through magnetic mirroring, unlike the azimuthal trapping of electrons seen in conventional Hall thrusters. These cusps, as well as the convergence of the field lines at the anode surface, meter the electron flow to the anode and create regions of efficient ionization of the propellant gas. Fuel is injected below the exposed anode tip at the base of the main channel. The distribution of cathode electrons throughout the discharge channel creates an electric field that accelerates singly- or multiply-ionized gas particles out of the thruster; the ions will be neutralized again by the cathode after imparting a reactive propulsive force to the thruster in the opposite direction. The DCF thruster operating on krypton at Stanford's vacuum facility is shown in the photograph in Fig. 3 a), while a close-up of a peculiar feature of the discharge – a toroid, or plasma "donut" located near the thruster exit plane – is shown in Fig. 3 b). The existence of this phenomenon is yet to be fully explained, although it is suspected to indicate a region of strong ionization.

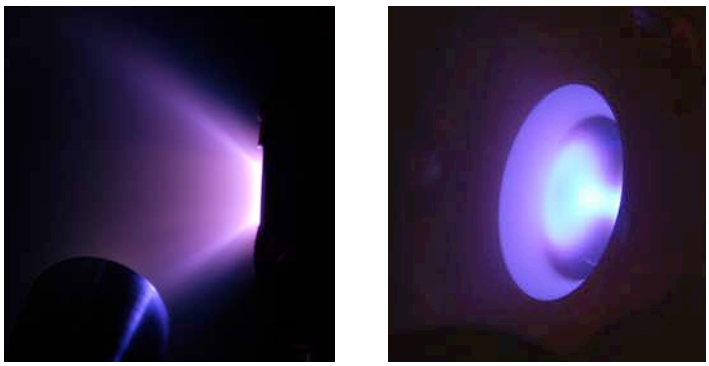

a) **b)**

Figure 3. a) DCF Thruster in operation on krypton at the Stanford Plasma Physics Laboratory. b) The plasma "donut" surmised to indicate a region of strong propellant ionization.

III. Results

A. Performance Testing

In order to obtain benchmark operating conditions for this new thruster, current-voltage (IV) profiles for several different flow rates of krypton were taken (see Fig. 4). The anode power supply was maintained in voltage-limited mode throughout the tests, with the electrical data read directly off the power supply (introducing the ~1% overestimation of the discharge current mentioned earlier). Voltage was scaled up and down to test for hysteresis in the thruster response, which is shown to be mostly negligible. However, in later testing care was taken to allow the thruster to come to equilibrium after making any changes to the operating conditions. The DCF thruster operates under a wide range of anode powers, varying from 27 W to over 230 W, with glow modes exhibited at values as low as 8 W. The anode efficiency, η_a, is defined as:

$$\eta_a \equiv \frac{T^2}{2\dot{m}P_a} \tag{2}$$

where T is the thrust, $\dot{m}$ is the mass flow rate to the anode, and P_a is the electrical power supplied to the anode. A point exists where the slope of the IV curve begins to approach zero: here, the thruster draws no additional current with increasing voltage to complete ionization of the propellant. In this case, we assume that there is no further gain in efficiency with the increase in power (other than perhaps, a reduction in divergence losses). Thus, it is advantageous to choose operating points at the onset of IV "plateaus," where the thruster draws just enough current to have efficiently ionized the propellant. Based on these criteria, we chose to use 8.2 sccm of flow with the anode potential set at 300 V (at which point the anode current was near 0.37 A) for the majority of our diagnostics, noting that this point falls near the middle of available flow rates and operating powers.

A variety of thrust performance experiments were carried out on the Stanford DCF thruster. First, the cathode was fixed to the thruster at an axial distance z of 2.8 cm (± 1 mm) away from the exit plane and a radial distance r of 3.85 cm (± 1 mm) away from the central thruster axis. In all performance tests, the cathode was pointed orthogonal to the thruster's central axis, parallel to the exit plane with the central axis of the cathode passing through the central axis of the thruster. Thrust data was taken at three different voltages for each of three flow rates: 10.5, 8.2, and 5.9 sccm of krypton propellant, giving nine distinct operating points. A variety of factors (nonlinearity in the thrust stand response and uncertainty in the precise orientation of the thruster, for example) contribute to uncertainty in the thrust measurement. We estimate the magnitude of this uncertainty to be within 20% of the measured value, and for the results that follow, only the measured value is reported (error bars are omitted for the sake of clarity). The resulting thrusts (in mN), calculated anode efficiencies η_a (given by Eq. (2)), and observed IV curves for the nine points are shown in Fig. 5. The IV curves from this test show excellent agreement with those obtained previously in Fig. 4, indicating repeatability in thruster operation. Our chosen point of 8.2 sccm, 300 V, and 0.36 A (in this case) is shown to yield a mid-range thrust of 4.9 mN with one of the highest efficiencies of 21.7%. Interestingly, the lowest flow rate of 5.9 sccm demonstrated some of the highest efficiency values measured, along with the expected lowest measured values of thrust. We also note one of the Stanford DCF thruster's most impressive operating points: 22.8% efficiency at an

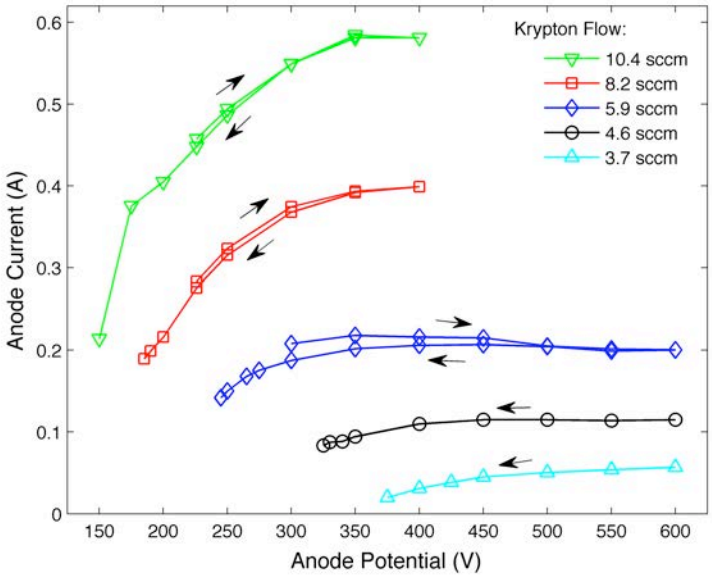

Figure 4. Current-voltage curves demonstrating DCF thruster operation over a variety of krypton flow rates and anode powers. The thruster was operated in voltage-limited mode.

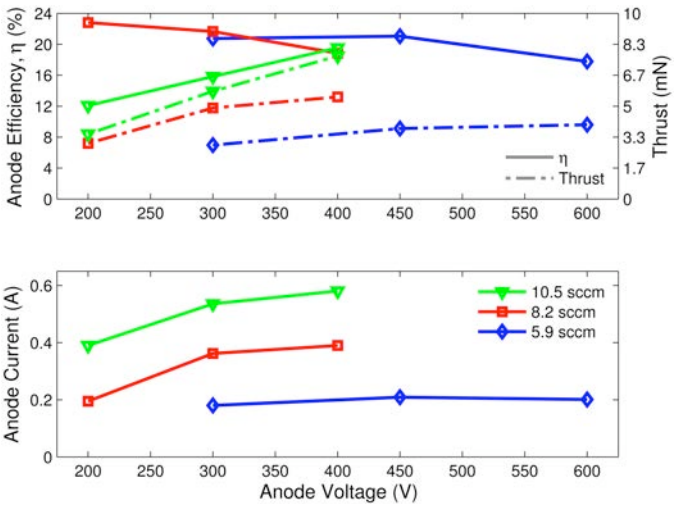

Figure 5. DCF thruster performance and operating points on krypton. The cathode was placed at *z* = 2.85 cm (±1 mm) and *r* = 3.85 cm (±1 mm).

anode power of only 39 W. Anode efficiencies over 20% are recorded up to 110 W, but above this threshold performance diminishes.

The cathode was then moved to an external mount to allow for the radial distance *r* to the central thruster axis to be varied at fixed axial distance *z*. The thruster remained on the thrust stand and translation stages, so we expect to slightly overestimate the thrust since thrust reductions associated with momentum transfer collisions between ions and the cathode body are not accounted for in this configuration. Two such studies were conducted over a range of radial positions (one test covered a greater spatial range, while the other included more tightly-spaced measurements) to discern the dependency of anode efficiency on cathode location. The operating point during both tests was 8.2 sccm of krypton flow at an anode potential of 300 V; the anode current varied between 0.35 A and 0.40 A as *r* was varied. The results are superimposed over a map of the near-field region of the DCF thruster along with simulated magnetic field lines calculated from Finite Element Method Magnetics (FEMM) software in Fig. 6. Measurements in both tests were taken at *z* = 3 cm (± 1 mm), which is indicated with an arrow to the scale of the drawing. Thruster performance data at the common spatial points of measurement between the two tests (3.0, 4.0, 5.0, and 6.0 cm) was, on average, within 2.2% of each other for the measured thrust, and within 5.6% of each other for the calculated efficiency, demonstrating the repeatability in operation of the DCF thruster. As indicated by the finely spaced data, thruster performance is highly dependent upon radial cathode position, with shifts in measured thrust of 14% and in calculated efficiency of almost 30% (relative) occurring in the span of a 0.25 cm change in cathode location. There is a general decrease in performance between 2.0 and 6.0 cm (with a few exceptions), which may be due to cathode electrons approaching the critical pitch angle (angle between an electron's velocity and the tangent to the magnetic field line that the electron is tracking) required for magnetic mirroring, the mechanism by which electron flow to the anode is metered. The highest region of efficiency is observed closest to the central axis, where one might expect to suffer the greatest losses from ion bombardment of the cathode in terms of both net thrust and cathode lifetime considerations.

Finally, the krypton performance characteristics of two different operating points (i.e. two different combinations of mass flow rate, discharge voltage, and discharge current) at a variety of cathode radial positions ranging from 3.0 cm and 6.0 cm were examined and compared to the existing data at 8.2 sccm and 300 V. The cathode axial position was set at 3 cm (± 1 mm) and oriented orthogonal to the thruster axis as discussed before, and suitable points were chosen from the better performing conditions from the data in Fig. 5. The results are summarized in Table 1.

The DCF thruster is shown to once again be repeatable in terms of required discharge power, with a deviation of around 4% compared with previous operation (Fig. 4) in both 5.9 sccm cases. The thrust measured, however, was generally lower than that seen previously at these points. The new measurements at the first and

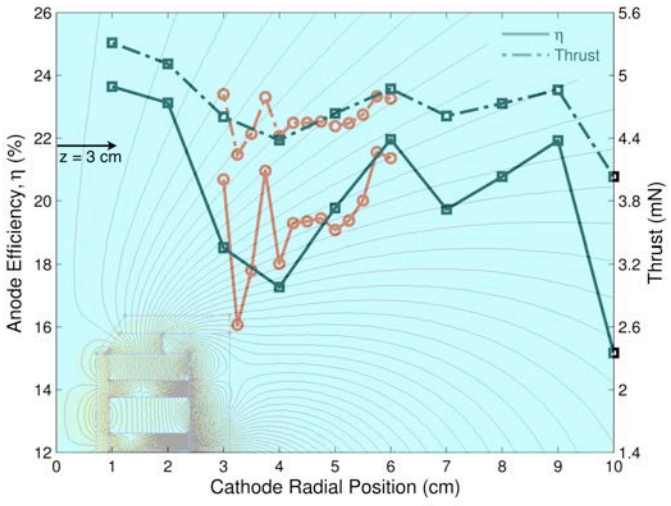

Figure 6. DCF thruster performance with varied cathode location, superimposed over the simulated magnetic field profile (FEMM). The cathode was scanned over *r* at fixed *z* = 3.0 cm (±1 mm).

second operating points (denoted "OP 1" and "OP 2" in Table 1) did indicate a performance dip with the cathode located near r = 4.0 cm – an effect also observed with the original operating point at 8.2 sccm of flow (see Fig. 6). We expect that further investigation of this region with a finer spatial sampling would demonstrate the strong dependency of thrust efficiency on cathode location as seen before. Understanding the sensitivity of the thruster to cathode position is imperative to optimize the DCF thruster for near 50 W and 100 W operation.

Table 1: Performance comparison between thruster operating points at varied radial cathode location.

Point / r (cm)	OP 1: 5.9 sccm, 300 V			OP 2: 5.9 sccm, 450 V			OP 3: 8.2 sccm, 300V		
	P_a(W)	T(mN)	η_a(%)	P_a(W)	T(mN)	η_a (%)	P_a(W)	T(mN)	η_a (%)
3.0	57	2.4	13.81	95	3.3	15.28	113	4.6	18.52
4.0	56	1.0	2.36	90	3.1	14.96	110	4.4	17.27
5.0	52	2.2	12.49	89	3.0	13.65	107	4.6	19.77
6.0	51	2.2	13.20	89	3.1	14.82	107	4.9	21.96

B. Probe Measurements

The DCF thruster underwent further diagnostic testing with a nude Faraday probe, as described previously.[13] The ion collecting area was 0.97 cm^2, and both the probe collector and guard ring were biased to -20 V for electron repulsion. Krypton propellant was used, with a flow rate of 8.2 sccm, and a discharge potential and current of 300 V, and 0.361 A, respectively. During the Faraday probe testing, the cathode was mounted to the thruster, and both were mounted on a rotating translation stage (see schematic in Fig. 1) with the axis of rotation positioned orthogonal to the intersection of the main thruster axis with the exit plane. The cathode was fixed at an axial distance of 2.8 cm (± 1 mm) and a radial distance of 3.85 cm (± 1 mm) (see Fig. 5 for performance data in this configuration). The probe remained stationary, oriented along the central axis of the thruster at a distance of 20.5 cm from the exit plane. The collected ion current density as a function of angular position relative to the central axis of the discharge is shown in Fig. 7 (the current density profile is fitted with a spline which is forced through zero at ±90°). The DCF thruster plume appears to be conically shaped with two main wings of high current density located at an average angle of 34° (as measured from the central axis), with a small swell in current density located along the thruster axis. This discharge profile qualitatively matches the one obtained by MIT[8]. The cathode is shown to have a significant effect on the plume, decreasing the width, angular position, and magnitude of the conical wing nearest to it. Further investigation is required to observe how widespread this effect is transmitted around the conical discharge, and the extent to which the ion current density in the plume is axisymmetric.

The beam currents (I_b) indicated on the diagram are calculated by assuming an axisymmetric plume and performing a stepwise volume-of-revolution numerical integration of the calculated spline fit according to:

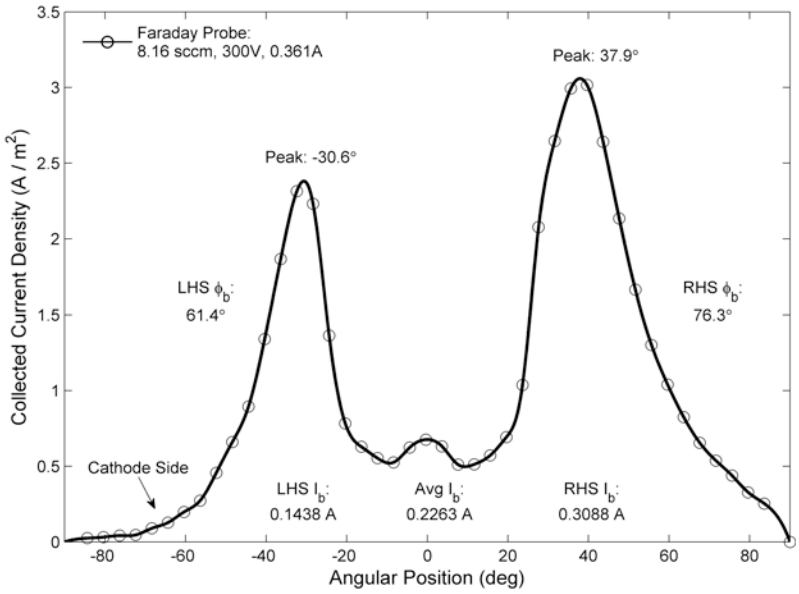

Figure 7. Ion current density collected over a sweep of the DCF thruster discharge. The spline fit is forced through zero at ± 90°. I_b represents the integrated beam current over the entire plume. φ_b is the angle corresponding to 95% of I_b for each half of the ion profile.

$$I_b = 2\pi R \int_0^{\pi/2} j(\phi)\sin(\phi)\,d\phi \tag{3}$$

where R is the distance from the thruster exit plane to the Faraday probe, j is the collected current density, and φ is the angular position relative to the thruster axis. Averaging the independent calculations from each wing yields an integrated beam current of 0.23 A, and thus an average beam efficiency (I_b/I_a) of 62.7%. The divergence angle of the observed plasma plume is estimated in two ways: calculating the angles of the maximum collected ion current and those encompassing 95% of the total beam current in each wing. The angles of maximum ion current are calculated to be 30.6° and 37.9° respectively for the cathode and opposite side, while the 95% beam currents are found to be respectively 61.4° and 76.3° (an almost 20% reduction in divergence angle due to the presence of the cathode). It is clear from Fig. 7 that the cathode certainly has a large effect on all of these plume characteristics.

A study was also carried out with the emissive probe to measure the plasma potential (φ_p) and electron temperature (T_e) throughout a horizontal plane passing through the center of the thruster exit plane and cathode. The thruster was kept in voltage-limited mode at 300 V, drawing an average of 0.354 A with a flow rate of 8.2 sccm of krypton. The cathode was fixed at an axial distance of 2.83 cm (± 1 mm) and radial distance of 3.0 cm (± 1 mm). Probe data was not taken where the cathode was located, or very near a protruding bolt on the exterior face of the thruster. The panels of Fig. 8 show the resulting spatial map in the plasma potential (top left) as well as the fluctuation (standard deviation) in the plasma potential (top right) arising as a result of the high frequency (~100 kHz) fluctuations seen in the hot probe potential. The plasma potential reaches a maximum of 100 V along the central axis near the exit plane (at r = 0 cm and z = 0.2 cm). The potential along the axis passes through a depression

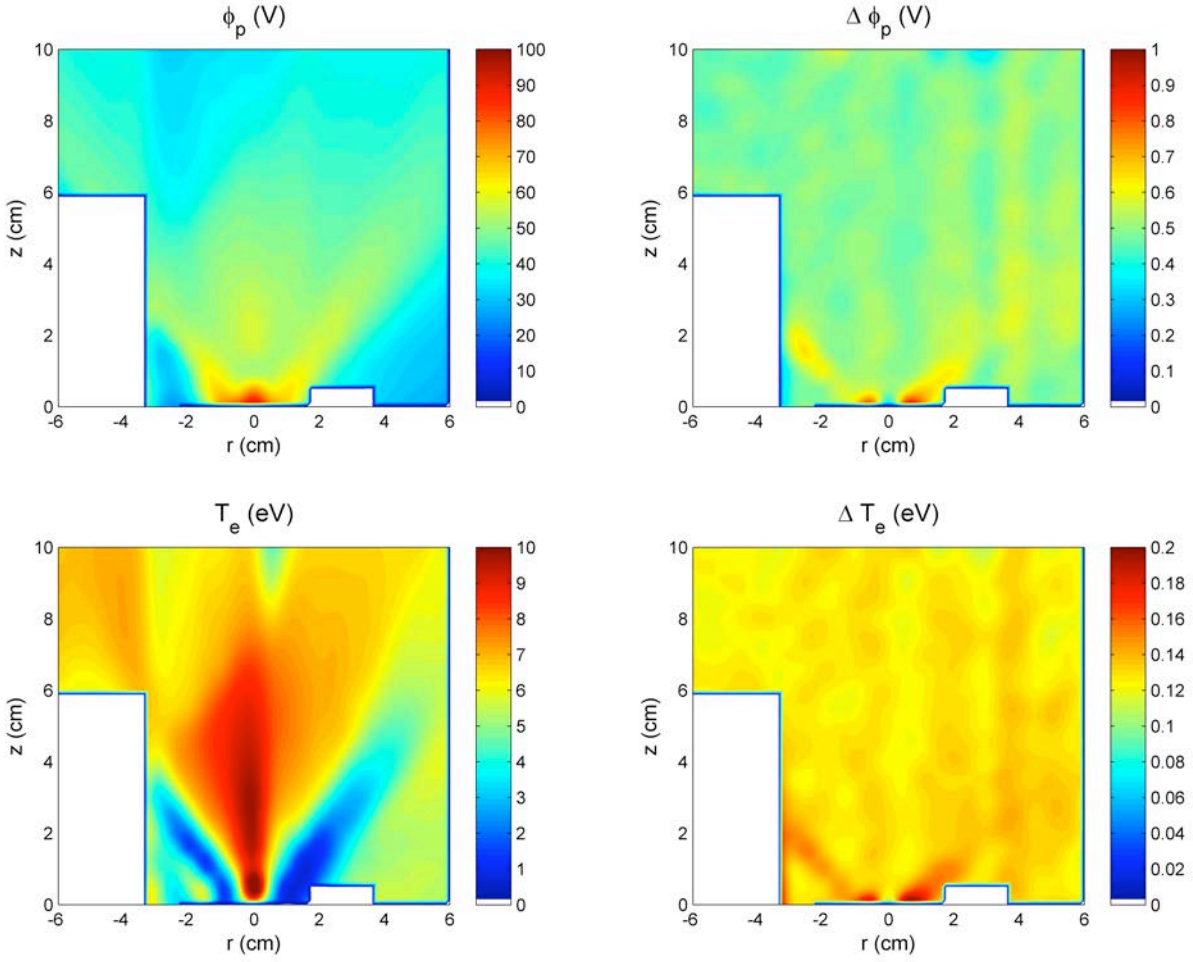

Figure 8. Floating plasma potential measurement and electron temperature calculation, with fluctuations (standard deviations), of the DCF thruster plume obtained with an emissive probe. The origin (0,0) is the intersection of the main thruster axis with the exit plane.

near 50 V at z = 1.0 cm, before increasing to more than 60 V at z = 2 cm and gradually diminishing to below 40 V at z = 6 cm. A distinct feature of the plasma potential measurement in this thruster is the relatively high potential region coinciding with the conical emission seen in the photographs (Fig. 3(a)) and the two peaks in the ion current trace (Fig. 7). The potential in these "wing" regions, can be as high as 70 V falling to less than 50 V at larger radial positions within the measurement domain. We note that the conical wing regions very near the exit plane are also a source of high frequency fluctuations, as apparent in the panel at top right; however, the standard deviation in this fluctuation is generally less than about 1 V.

The observed plasma potential and cold-probe floating potential (not shown) is used to determine the electron temperature in the near-field (see bottom-left panel in Fig. 8), calculated from the model given in Eq. (1). The conical plume, generally of high plasma potential, appears to be a region low in electron temperature. Also apparent is the presence of a large jet of high electron temperature plasma that is ejected throughout the interior region of the plume. This region of elevated electron temperature along the thruster axis is concomitant with the region of increased plasma potential near the centerline. The lower right panel of Fig. 8 depicts fluctuations (standard deviation) in electron temperature computed from the measured fluctuations in hot and cold probe signals. The magnitude of the maximum fluctuations in plasma potential and electron temperature are ~1% and ~2% of the mean (time-averaged) values, respectively.

C. Alternate Modes

In addition to the operating conditions and performance data mentioned previously, the DCF thruster exhibited numerous irreproducible operating modes that resulted in both unusually high and low thrust efficiencies. One notable high-current mode (which has, as yet, been elusive to reproduction) resulted in anode efficiencies well above 30% in an operating range of 160 W to 180 W at the 8.2 sccm, 300 V point used continuously throughout our testing. Further investigation is ongoing to recreate the operating conditions of this mode. In addition, unusually low anode efficiency values were obtained (at similar operating conditions to those shown in Fig. 5), especially at a cathode radial location of 5.5 cm. The explanation for the poor performance at this location (still irreproducible after early tests) is the subject of current research. An example of this phenomenon is demonstrated in the ion current densities of Fig. 9; one might assume from the ion profiles that the point at r = 5.5 cm is more efficient, yielding more ion current. Yet, it is in fact the opposite. Because of uncharacteristically low thrust, the 5.5 cm point has a very low specific impulse (I_{sp}) of 440 s, compared to the 980 s of the 3.85 cm point, making the latter point much more efficient. These data, taken for a range of operating points during this relatively poor mode of thruster operation demonstrates the "squeezing" effect that the cathode imposes on the discharge plume We note that the center and far wing of the r = 3.85 cm discharge matches very well with the r = 5.5 cm trace where the cathode is farther away, yet the closer wing is vastly reduced in both extent and total beam current. This result suggests that the cathode placement and overall electron emission efficiency may be a very influential means of tuning the divergence and intensity of the plasma plume.

IV. Conclusion

We present the first experimental results of a diverging cusped field (DCF) thruster with a straight-walled channel. This study is motivated by the recent interest in cylindrical variants of Hall thrusters, and in particular, the recent successes of a cusped field thruster fabricated at MIT with a geometrically diverging wall. The thruster variant described here retains some key features of the MIT design – a decreasing magnetic field downstream along the axis and somewhat diverging cusps within the channel – but dispenses with the diverging channel wall geometry. Various measurements on krypton between 25 and 250 W indicate qualitative similarities between the plasma discharge and operating behaviors of the Stanford and MIT DCF thrusters, suggesting that the ion divergence of the plume is more closely connected to the magnetic

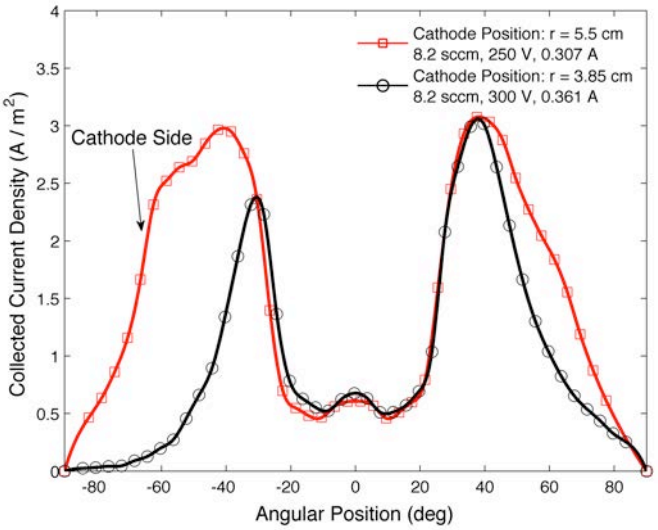

Figure 9. Two ion current density profiles at differing radial cathode locations. The influence of the cathode is clearly seen on the left side of the discharge.

field structure than to the channel geometry. Various performance metrics (thrust, specific impulse, and anode efficiency) are found to be very sensitive to cathode placement. Thrust efficiencies as high as 23% are demonstrated, particularly at low powers (40 W). Discharge current measurements confirm that these DCF thrusters are unusually quiescent, and do not depict instabilities during ionization that are often seen in their Hall thruster counterparts. An emissive probe is used to obtain maps of the plasma potential in the near-field, indicating that the regions strong in visible emission appear to coincide with areas of relatively high plasma potential. Surprisingly, the electron temperature is quite low in these regions, but the central core of the discharge yields a region of high electron temperature that exceeds 10 eV in some areas. Future studies will utilize the measured plasma potential data as a basis for kinetic simulations of cathode-emitted electrons, aiding in an understanding of the electron temperature structure seen to date, as well as more general thruster operating principles.

Acknowledgments

This research is supported by the Air Force Office of Scientific Research, with Dr. Mitat Birkan as the Program Manager. Support for C.V.Y. was provided by the Summer Undergraduate Research Institute (SURI) through the School of Engineering and the Office of the Vice Provost at Stanford University.

References

[1]Hruby, V., Monheiser, J., Pote, B., Freeman, C., and Connoly, W., "Low Power Hall Thruster Propulsion System," *26th International Electric Propulsion Conference*, Kitakyushu, Japan, Oct. 1999, pp. 544-551.

[2]Ito, T., Gascon, N., Crawford, W.S., and Cappelli, M.A., "Experimental Characterization of a Micro-Hall Thruster," *Journal of Propulsion and Power*, Vol. 23, No. 5, Sept-Oct 2007, pp. 1068-1074.

[3]Raitses, Y., Fisch, N. J., "Parametric investigations of a nonconventional Hall thruster," *Physics of Plasmas*, Vol. 8, No. 5, May 2001, pp. 2579-2586.

[4]Smirnov, A., Raitses, Y., Fisch, N. J., "Enhanced ionization in the cylindrical Hall thruster," *Physics of Plasmas*, Vol. 95, No. 2, 15 Jul. 2003, pp. 852-857.

[5]Smirnov, A., Raitses, Y., Fisch, N. J., "Experimental and theoretical studies of cylindrical Hall thrusters," *Physics of Plasmas*, Vol. 14, No. 5, 057106, 2007.

[6]Matlock, T. et al., "Spectroscopic and Electrostatic Investigation of the Diverging Cusped-Field Thruster," *45th AIAA/ASME/SAE/ASEE Joint Propulsion Conference*, Denver, CO, Aug. 2009.

[7]Gildea, S., Batishchev, O., Martinez-Sanchez, M., "Fully Kinetic Modeling of Divergent Cusped Field Thrusters," *45th AIAA/ASME/SAE/ASEE Joint Propulsion Conference*, Denver, CO, Aug. 2009.

[8]Courtney, D. G., "Development and Characterization of a Diverging Cusped Field Thruster and a Lanthanum Hexaboride Hollow Cathode," Masters Thesis, Dept. of Aeronautics and Astronautics, Massachusetts Institute of Technology, Cambridge, MA, 2008.

[9]Hargus, W. A., "Investigation of the Plasma Acceleration Mechanism Within a Coaxial Hall Thruster," Ph.D. Dissertation, Mechanical Engineering Dept., Stanford University, Stanford, CA 2001, pp. 37-39.

[10]Smith, A, W., and Cappelli, M. A., "Time and Space-correlated plasma potential measurements in the near field of a coaxial Hall plasma discharge," *Physics of Plasmas*, Vol. 16, 2009, 073504.

[11]N. Hershkowitz, "Plasma Diagnostics, Vol. 1 Discharge Parameters and Chemistry," Eds. by O. Auciello and D.L. Flamm, Academic Press, New York, 1989.

[12]Hargus, W. A., "Investigation of the plasma acceleration mechanism within a coaxial Hall thruster," Ph.D. Thesis, Mechanical Engineering Department, Stanford University, 2001.

[13]Hofer, R. R., Walker, M. L. R., Gallimore, A. D., " Comparison of Nude and Collimated Faraday Probes for use with Hall Thrusters," *27th International Electric Propulsion Conference*, Pasadena, CA, Oct. 2001.